The conformations of monensin-A metal complexes in solution determined by NMR spectroscopy

Tamas Martinek,[a] Frank G. Riddell,[b] Craig Wilson[b] and Charles T. Weller[c]

[a] *Institute of Pharmaceutical Chemistry, Albert Szent Gyorgyi Medical University, Szeged, Hungary*
[b] *School of Chemistry and* [c] *School of Biomedical Sciences, The University of St Andrews, St Andrews, Scotland, UK KY16 9LT*

Received (in Cambridge, UK) 4th October 1999, Accepted 1st November 1999

The structures in solution of the Na^+, K^+ and Rb^+ salts of monensin have been determined by the use of NOESY distance restraints and molecular modelling. The structures are similar to those obtained by X-ray diffraction with the exception of a close carboxylate oxygen-to-metal distance and only five observed close metal-to-oxygen ligating interactions. Molecular dynamics involving the derived structure of the sodium salt at increasing relative permittivity sheds light on the mechanism by which monensin binds to and unbinds from sodium ions in the membrane surface. The series of structures as the size of the metal ion increases also shows that the whole monensin molecule adapts to incorporate changes in the ionic radius including changes in torsion angles, changes in heterocyclic ring conformations and changes in the ligation and hydrogen bonding patterns.

Introduction

The ionophoric antibiotics are materials that continue to attract considerable interest. Their role is to mediate membrane transport of the alkali metal ions and as a consequence they have considerable biological activity.[1]

Monensin, (**1**) an ionophoric antibiotic isolated from *Streptomyces monensis*, with a preference for complexing sodium, is amongst the most widely investigated. Monensin is used commercially as a coccidiostat for poultry.

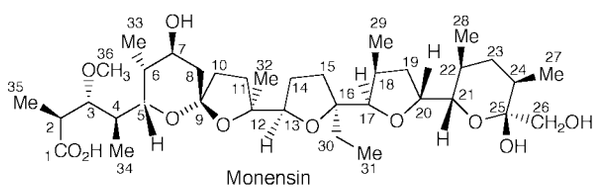

1

There are two main items of chemical interest concerning the ionophoric antibiotics. The first is their membrane behaviour: the kinetics and mechanism of the transport process and the membrane stability of the complex. The second is the molecular structure of the complex and the way that it influences the kinetics, mechanism and stability in the membrane. Monensin has featured strongly in both types of study.

NMR studies of the kinetics and mechanism of monensin-mediated transport in model phospholipid bilayers[2–4] have shown that one monensin molecule transports one alkali metal ion through the membrane, that dissociation of the complex is the rate determining step and that the sodium complex is more stable in the membrane than the potassium or lithium complexes. Although in the absence of Na^+ ions, K^+ is transported more rapidly due to a faster dissociation rate, the greater stability of the Na^+ complex means that in the presence of both ions Na^+ is transported preferentially.

Monensin is the ionophoric antibiotic for which the most crystallographic data is available. For monensin A (**1**) the structures of the free acid,[5] the hydrated and anhydrous forms of the Na^+ complex,[6] the NaBr complex,[7] the Ag^+ complex,[8] and the hydrated K^+ complex,[9] have been determined. For monensin B (**1**, replace C(30) and (31) by methyl) structures for the monohydrate of the Na^+ complex[10] and the Li^+ and Ag^+ salts,[11] have been determined. In more recent years the ability of NMR spectroscopy combined with molecular modelling including NMR derived distance restraints to determine molecular structures in solution has been applied to the ionophoric antibiotics[12,13] and in particular to sodium monensin.[14] Two advantages of the NMR method are its ability to simulate molecular dynamic processes and the fact that, unlike solid state methods, it deals with isolated molecules in solution. A disadvantage is that it depends upon molecular modelling which in turn is critically dependent upon the force field employed.

The structures reported for the monensin derivatives by both X-ray crystallography and NMR are similar. The metal ion in all cases seems to be at the centre of a distorted octahedron of ether and hydroxy oxygen atoms (O(4), O(6), O(7), O(8), O(9) and O(11)) whilst the hydroxy groups on O(10) and O(11) hydrogen bond to the two carboxylate oxygen atoms O(2) and O(1) respectively. Interestingly, but almost not remarked on in the above work, there seems to be no close contact between the positively charged metal ion and the negative carboxylate group in all the structures reported. By contrast in the silver salt of nigericin, X-ray crystallography shows a close contact between the carboxylate group and the silver ion.[15]

Whilst the static pictures of monensin derivatives obtained from X-ray crystallography are of great interest in that they show the way in which the metal ions are co-ordinated and some of the ways that the ligand changes in order to accommodate ions of different sizes, they do not assist very much in the understanding of the mechanisms by which the hydrated metal ions are taken into the complex and the way in which the complex releases the metal ion back to the aqueous solution. It has been suggested[3] that the ionised ionophore molecule sits near the membrane surface with the carboxylate group projecting into the aqueous medium. The first step is the association of the metal ion with the carboxylate as one water molecule is lost, and subsequently the ether and hydroxy oxygens along the molecule replace the remaining water molecules in sequence. An alternative mode has been suggested, based upon the crystallographic results, in which O(7) is the first atom in the monensin

Table 1 Ionic radii of the alkali metals[a]

M^+	*r*/pm	% increase
Li^+	76	—
Na^+	102	34
K^+	138	35
Rb^+	152	10
Cs^+	167	10

[a] Taken from reference 18 (refers to octahedral co-ordination).

molecule to associate with the metal ion and the other oxygens sequentially replace water around the metal ion.[6] Whilst both models have sequential complexation by adjacent oxygens the difference between them is substantial. In the first model the complexation starts at one end of the molecule and proceeds along it. For the second the complexation starts in the middle of the molecule and spreads out in both directions. In principle dynamic molecular modelling studies based upon NMR or X-ray derived structures should be able to resolve which one occurs.

In addition, a coherent study of the structures of the monensin complexes as the radius of the metal ion is increased from Li^+ to Rb^+ should provide clear evidence of the regions of the molecule in which there is sufficient flexibility to facilitate the folding and unfolding processes. The ionic radii of the alkali metals are given in Table 1. This table also shows the % change in ionic radius at each step down the group. Thus the changes in size from Li^+ to Na^+ and from Na^+ to K^+ are much more important than change from K^+ to Rb^+.

Results and discussion

The NMR samples were prepared by vigorously stirring a $CDCl_3$ solution of sodium monensin with a saturated aqueous solution of the metal carbonate. The carbonates were chosen because their high solubility in water should boost a mass action effect to exchange the metal ion. The $CDCl_3$ layer was then separated and filtered into the NMR tube through a short column of the anhydrous metal carbonate. In the case of the potassium derivative in excess of 90% exchange was achieved and for the rubidium derivative in excess of 95% was achieved.

The assignment of the ^1H NMR spectrum of the monensin salts was straightforward. The resonance for H(20) was readily identified in the 1D ^1H spectrum at *ca.* 4.40 ppm. Starting from this resonance the use of COSY connectivities gave most of the assignments in rings D and E (ring numbering A–E runs from left to right in structure **1**). NOESY spectra enabled the assignment and differentiation of the C(26) geminal pair. The resonance at around 4.0 ppm was then readily assigned as H(5) from the COSY connectivities which then allowed the assignment of the resonances from ^1H on C(2) to C(8). The CH_2 groups on ring B form an isolated spin system which can be distinguished by a 2D HSQC experiment at natural abundance. The remaining resonance in the ether region must belong to H(13) which then gives the assignments in ring C. These assignments were then checked against the assignments given in reference 16 and satisfactory agreement was found. Chemical shifts are given in Table 2.

The monensin salts in this paper are roughly globular molecules with a relatively low molecular weight (NaMon = 693 amu) and molecular tumbling correlation times in the ns region. Consequently they produce rather low intensity cross peaks and so optimisation of the signal to noise ratio (S/N) in the NOESY spectra assumes a special importance. NOESY spectra were obtained with mixing times of between 100 and 700 ms. The nOe build up rates proved to be essentially linear in the 0–400 ms range. The longer mixing times produced a levelling off in peak intensity. The NOESY cross peak intensities at 400 ms were then adopted as a compromise between acceptable S/N and linearity for the establishment of distance restraints.

Table 2 ^1H chemical shifts (δ_H) of the alkali metal complexes of monensin

	δ_H		
Atom	Na	K	Rb
2	2.55	2.59	2.55
3	3.20	3.25	3.27
4	2.08	2.15	2.13
5	4.05	3.94	3.77
6	2.24	2.17	2.26
7	3.90	3.87	3.86
8B	1.91	1.90	1.89
8B	1.70	1.76	1.76
10A	2.01	1.93	2.01
10B	1.70	1.59	1.69
11A	2.02	2.00	1.91
11B	1.72	1.67	1.67
13	3.55	3.52	3.47
14A	1.78	1.72	1.70
14B	1.57	1.64	1.61
15A	2.30	2.28	2.21
15B	1.47	1.45	1.61
17	3.96	3.92	3.92
18	2.26	2.30	2.33
19A	2.19	2.27	2.23
19B	1.56	1.45	1.42
20	4.42	4.40	4.35
21	3.85	3.91	3.93
22	1.38	1.30	1.30
23A	1.44	1.47	1.38
23B	1.32	1.39	1.28
24	1.48	1.51	1.49
26A	4.00	3.97	3.91
26B	3.31	3.41	3.40
27	0.86	0.86	0.86
28	0.82	0.86	0.88
29	0.91	0.93	0.94
30A	1.60	1.60	1.62
30B	1.51	1.51	1.48
31	0.96	0.86	0.91
32	1.53	1.51	1.48
33	0.94	0.94	0.93
34	1.21	1.14	1.09
35	1.25	1.25	1.25
36	3.38	3.39	3.34

Distances were calculated using the isolated spin pair approximation (ISPA) which applies, and serves as a reliable distance estimation for the restrained molecular dynamics (MD) calculations in this case. The reference distance was taken from the cross peaks of the geminal pair on C(26), assumed to be 1.78 Å as determined crystallographically. The distance classification method was then used with NOEs being classified as very strong (100–180 pm), strong (180–270 pm), medium (180–330 pm) or weak (180–500 pm). A list of the experimental distances as deduced from the NOESY integrals, the applied restraints and back-calculated distances in the final model is given in Table 3. Agreement between the observed and calculated distances from the models is particularly good at short distances and satisfactory for the longer distances where accurate integration of the NOESY cross peaks becomes more difficult. Back-calculated distances are from averaging over the entire time course of a 100 ps molecular dynamics simulation using the NOESY distance restraints.

The starting model was taken from the structure of the sodium salt[6] obtained from the Cambridge Crystallographic Data Centre to which were added hydrogen atoms to fill the vacant valencies. For the non-sodium-containing salts the sodium structure was used with the appropriate metal ion replacing sodium directly. The initial conformational set was created by high temperature molecular dynamics and sub-

Table 3 Observed distances (Å) from NOESY spectra of M^+ monensin salts, applied restraints and back-calculated distances

Na					K					Rb				
Proton pair		Exp. dist./Å	Upper boundary/ Å	Back calc. dist./Å	Proton pair		Exp. dist./Å	Upper boundary/ Å	Back calc. dist./Å	Proton pair		Exp. dist./Å	Upper boundary/ Å	Back calc. dist./Å
H21	H20	2.4	2.7	2.2	H21	H20	2.2	2.7	2.3	H21	H20	2.5	2.7	2.3
H191	H20	2.3	2.7	2.4	H191	H20	2.3	2.7	2.3	H192	H20	3.1	3.3	3.2
Me29	H20	2.9	3.3	2.6	Me29	H20	2.8	3.3	3.0	H191	H20	2.2	2.7	2.3
Me28	H20	2.7	3.3	2.8	Me28	H20	2.6	2.7	2.7	H22	H20	2.9	3.3	2.9
H192	H20	3.2	3.3	3.3	H192	H20	2.9	3.3	3.4	Me29	H20	2.7	3.3	3.0
H6	H5	2.2	2.7	2.2	Me32	H5	3.6	5.0	3.3	Me28	H20	2.4	2.7	2.6
H4	H5	2.9	3.3	2.8	Me34	H5	3.4	5.0	3.0	H231	H21	2.4	2.7	2.5
Me32	H5	3.3	3.3	3.1	H261	H262	1.8	1.8[a]	1.8	Me28	H21	2.7	2.7	2.8
Me34	H5	2.9	3.3	3.1	Me27	H262	2.8	3.3	2.9	H261	H262	1.8	1.8[a]	1.8
H261	H262	1.8	1.8[a]	1.8	H18	H17	2.0	2.7	2.2	H18	H17	2.1	2.7	2.2
Me27	H262	2.9	3.3	2.9	H192	H17	2.4	2.7	2.5	H192	H17	2.4	2.7	2.5
H18	H17	2.0	2.7	2.2	H3	H5	3.6	5.0	2.9	H301	H17	2.7	2.7	2.7
H192	H17	2.7	2.7	2.5	Me33	H5	3.8	5.0	4.4	Me31	H17	2.7	2.7	2.7
Me31	H17	3.2	3.3	2.8	H6	H7	2.3	2.7	2.4	H6	H7	2.3	2.7	2.3
H3	H5	3.7	5.0	3.0	H82	H7	2.3	2.7	2.3	H82	H7	2.2	2.7	2.3
Me33	H5	3.8	5.0	4.4	H81	H7	2.5	2.7	2.5	H81	H7	2.4	2.7	2.5
Me29	H17	4.3	5.0	4.5	Me33	H7	2.7	3.3	2.8	Me33	H7	2.7	2.7	2.7
H6	H7	2.5	2.7	2.4	H231	H21	2.5	2.7	2.5	H22	H21	2.9	3.3	2.8
H82	H7	2.4	2.7	2.3	Me28	H21	2.9	3.3	3.0	Me33	H82	2.7	3.3	3.1
Me33	H7	2.8	3.3	2.8	H142	H13	2.1	2.7	2.3	Me32	H5	3.5	5.0	3.2
H231	H21	2.6	2.7	2.5	Me31	H13	2.9	3.3	3.0	Me34	H5	2.9	3.3	3.0
Me28	H21	3.0	3.3	3.0	H3	Me36	2.7	2.7	2.7	H4	H5	2.9	3.3	2.8
H152	H13	2.6	2.7	3.0	H4	Me36	2.8	3.3	2.9	H142	H13	2.1	2.7	2.3
Me32	H13	2.9	3.3	3.1	Me35	Me36	4.4	5.0	4.5	H141	H13	2.3	2.7	3.2
Me31	H13	3.2	3.3	3.3	Me33	Me36	3.9	5.0	4.0	Me32	H13	2.8	3.3	2.9
H3	Me36	3.3	3.3	2.8	H24	H261	2.3	2.7	2.4	Me31	H13	3.1	3.3	3.1
H4	Me36	3.0	3.3	2.8	H2	H3	3.4	5.0	2.9	Me35	H5	3.8	5.0	5.4
Me35	Me36	4.6	5.0	4.6	Me35	H3	2.9	3.3	3.2	H5	Me33	3.7	5.0	4.4
Me33	Me36	4.1	5.0	4.1	Me33	H3	3.0	3.3	3.2	H6	H3	2.1	2.7	2.1
H24	H261	2.6	2.7	2.3	Me35	H2	2.7	2.7	2.6	H4	H3	2.3	2.7	2.4
H2	H3	3.0	3.3	2.8	Me34	H2	2.7	2.7	2.6	Me35	H3	2.8	3.3	3.1
H6	H3	2.1	2.7	2.1	H142	H152	2.4	2.7	2.5	Me34	H3	3.7	5.0	4.5
H4	H3	2.5	2.7	2.4	Me29	H152	2.3	2.7	2.8	Me33	H3	2.9	3.3	3.1
Me35	H3	3.1	3.3	3.1	H22	H191	2.7	2.7	2.7	Me35	H2	2.6	2.7	2.6
Me33	H3	3.3	3.3	3.1	Me34	H4	3.2	3.3	2.7	Me34	H2	2.4	2.7	2.6
Me35	H2	2.8	3.3	2.6	Me33	H4	2.4	2.7	2.7	Me34	H4	2.5	2.7	2.8
Me34	H2	2.7	3.3	2.8	H111	H112	1.8	1.8[a]	1.8	Me33	H4	2.4	2.7	2.7
H142	H152	2.3	2.7	2.5	H81	H82	1.8	1.8[a]	1.8	Me34	Me32	3.2	3.3	3.5
H151	H152	1.8	2.7	1.9	Me33	H82	2.8	3.3	3.1	Me29	H191	2.6	2.7	3.0
Me29	H152	2.5	2.7	3.1	Me34	Me32	3.6	5.0	3.9	Me31	Me32	3.2	3.3	3.6
H192	H191	1.9	2.7	1.8	Me27	H24	2.7	3.3	2.7	Me32	H112	2.8	3.3	3.0
H22	H191	2.4	2.7	2.6	Me29	H191	2.6	2.7	2.9	H101	H102	1.8	1.8[a]	1.8
Me34	H4	3.1	3.3	2.7	H22	H20	2.8	3.3	2.9	H261	Me27	3.7	5.0	5.4
Me33	H4	3.0	3.3	2.8	Me35	H5	4.1	5.0	5.4	H262	Me27	2.9	3.3	2.8
H81	H82	2.0	2.7	1.8	Me34	Me36	4.6	5.0	5.5	Me36	H4	3.0	3.3	2.8
Me33	H82	3.4	5.0	3.1	Me32	H13	2.8	3.3	3.0	Me36	Me35	4.2	5.0	4.6
H142	H141	2.2	2.7	1.8	Me27	H261	3.5	5.0	4.6	Me36	Me34	4.9	5.0	5.3
Me34	Me32	3.7	5.0	3.6	Me27	H262	2.8	3.3	2.9	Me36	Me33	3.9	5.0	4.0
Me27	H24	2.8	3.3	2.7	H24	H261	2.3	2.7	2.4	H24	H261	2.4	2.7	2.4
Me29	H191	2.9	3.3	3.0										
Me32	H112	2.7	2.7	2.9										
H13	H111	[b]	3.3	2.6										
Me27	H262	3.6	3.3	2.9										
Me27	H261	3.9	5.0	4.5										
H24	H261	2.5	2.7	2.3										

Lower bounds for distance restraints were 1.8 Å except for cases [a] where they were 1.0 Å. [b] The upper limit was estimated from the peak height due to partial overlap with an exchange cross peak. Back-calculated distances are from averages over the entire time course of a 100 ps molecular dynamics simulation using the NOESY distance restraints.

sequent rapid quenches. Using the starting model 50 ps MD simulation was performed at 1000 K with 1 fs time steps. The resulting conformations were minimised and saved at every 1000 steps. This simulation was run without restraints and was expected to probe the whole of the conformational space available for each of the monensin salts thus providing random initial conformations. In each case the 50 quenched conformations and the starting model form the initial structure set of 51 members.

As in every molecular mechanics or molecular dynamics simulation the results depend critically on the choice of the force field. The classical force fields in common use for structure determination from NMR data are designed for and parameterised for proteins, nucleic acids and carbohydrates and so may not be optimal for ionophoric systems with their associated metal ions. Second generation, *e.g.* consistent valence force field (CVFF) and rule based, *e.g.* extensible systematic force field (ESFF) force fields cover a wider range of functional groups and so may be more appropriate for ionophores. Of these two approaches the ESFF attempts to provide the widest possible coverage of the periodic table with reasonable accuracy. ESFF has been used, for example, to model proteins containing

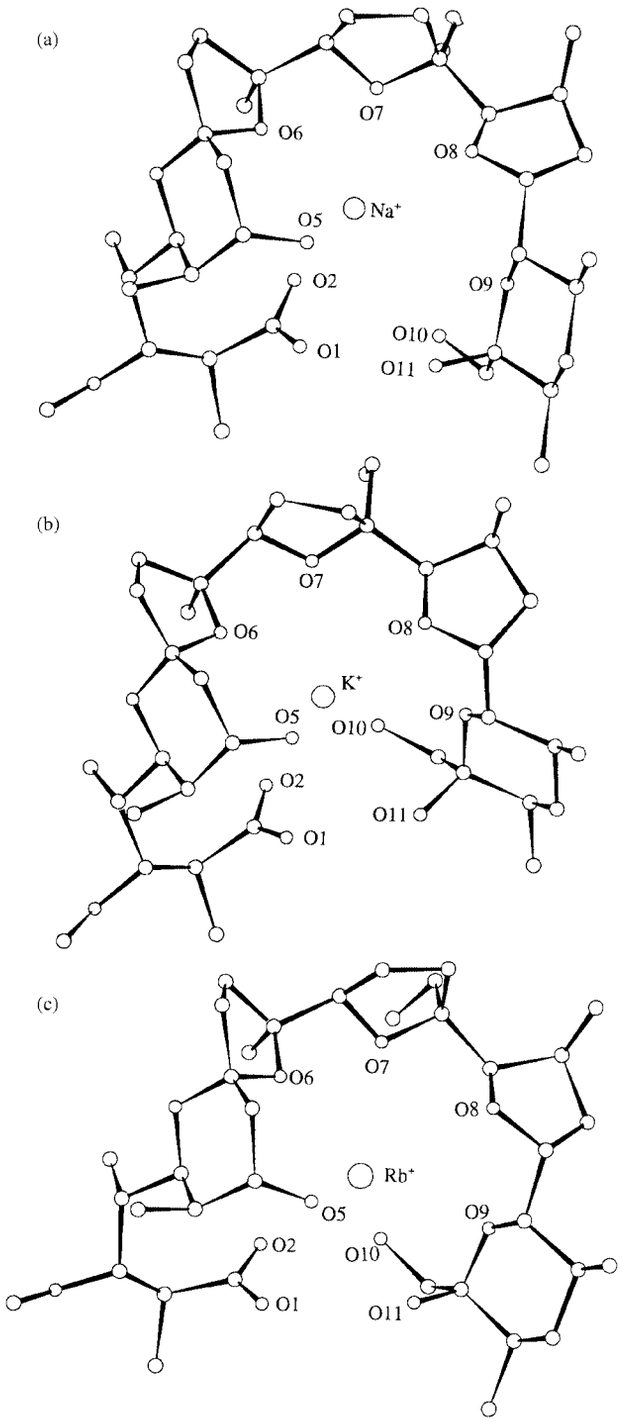

Fig. 1 Final typical minimum energy molecular structures for the sodium salt (a), potassium salt (b) and rubidium salt (c) of monensin.

metals. In our previous work on the ionophoric antibiotic, sodium tetronasin,[13] we found that the ESFF force field was much better than the CVFF force field in that the CVFF force field failed to retain the metal ion in the structure even with a relative permittivity of 1 to emphasise the charge–charge interaction. Accordingly we chose to use the ESFF force field for the current study.

For all the salts studied here the simulated annealing (SA) protocol used the random initial conformations, started at 900 K and finished at 10 K. The temperature step was set at 40 K from 900 to 500 K and 10 K from 500 to 10 K. The duration of the steps was 500 fs from 900 to 500 K and 313 fs from 490 to 10 K. A distance-dependent relative permittivity (ε) was initially employed for these SA calculations in which the relative permittivity was scaled proportionately to the charge separation.

Table 4 Representative metal ion–oxygen distances (Å) in the low energy conformations

	d/Å		
	Na	K	Rb
O(2)	2.57	2.79	2.92
O(1)	3.02	3.09	3.40
O(5)	2.60	2.89	2.99
O(6)	2.61	2.86	2.95
O(7)	2.57	2.89	2.91
O(8)	2.87	2.78	3.11
O(9)	3.56	3.20	3.17
O(10)	3.52	3.46	3.34
O(11)	3.85	3.44	2.94

The ESFF force field kept the metal ions in the proximity of the oxygen atoms and in each case produced several low energy 'cage-like' conformations with the metal ion in the centre. These low energy structures were similar to the starting X-ray structure of the Na^+ salt with the exception that there was a close contact between one of the carboxylate oxygens O(2) and the metal ion. For example in the case of the sodium salt there was only one weak hydrogen bond between the O(10) and the O(1) carboxylate oxygen (O · · · H distance = 222 pm) as opposed to two in the solid state structures. The sodium is close to (<290 pm) O(2), O(5), O(6), O(7), O(8) and has a relatively close contact with O(1) (302 pm).

This difference between the X-ray structures and the NMR structures could arise from several causes: (1) the solution structure is different from the solid structure due to "crystal packing effects", (2) the dielectric constant protocol we are using overemphasises charge–charge interactions, (3) the models might not be in the global energy minimum, (4) the ESFF force field may inherently overemphasise charge–charge interactions at the expense of hydrogen bonds. However, the ESFF force field treats hydrogen bonds as a natural consequence of the standard van der Waals and electrostatic parameters so this is unlikely to be the cause.

For isolated molecules in solution the choice between different conformational (or constitutional) energy minima depends upon intramolecular forces. In the solid state intermolecular forces become important and can, in appropriate cases, provide sufficient extra influence to allow the molecule to adopt a conformation that is not the solution minimum. This is what is commonly referred to as the influence of "crystal packing forces". Evidence from our own work suggests that energy differences of up to 6 kJ mol^{-1} can be overcome this way.[17] It seemed to us that this could explain what is happening here. Nevertheless it was decided to test the matter further.

We re-ran the SA of the sodium salt under several different sets of conditions. First the relative permittivity was fixed at 4, close to that in ether-like compounds and similar structures were obtained. Next we fixed the distances between Na^+ and O(5), O(6), O(7) and O(8) to those found in the first SA calculations and then allowed the O(2)-to-sodium distance to vary in the SA. Similar structures to the earlier SA results with short Na^+-to-O(2) distances were found. We then fixed the O(2)-to-sodium distance to that found in the crystallographic studies and repeated the SA. Structures of appreciably higher energy were obtained. The structures thus seem not to be due to a relative permittivity effect nor to being trapped in a false energy minimum. We conclude that the short carboxylate-to-metal distances are a genuine feature of the molecules free in solution because it is unlikely that the ESFF force field will overstate charge–charge interactions and understate hydrogen bonding.

Low energy conformations in which the oxygens close to the metals are marked are shown in Fig. 1. Representative metal-to-oxygen distances from the structures are given in Table 4. The

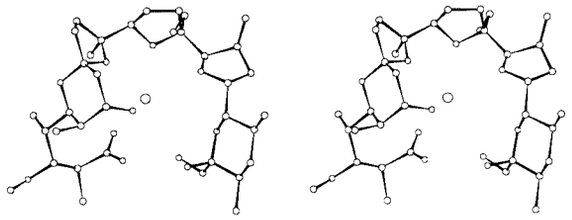

Fig. 2 Stereoview of a typical minimum energy molecular structure for the sodium salt of monensin.

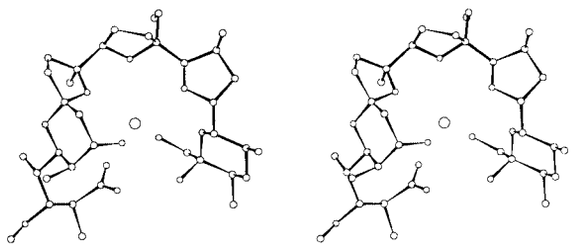

Fig. 3 Stereoview of a typical minimum energy molecular structure for the potassium salt of monensin.

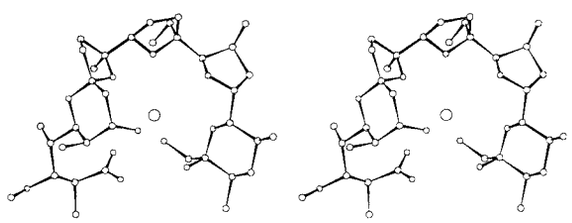

Fig. 4 Stereoview of a typical minimum energy molecular structure for the rubidium salt of monensin.

structures of representative low energy conformations of the salts are presented as stereoviews in Figs. 2–4.

Comparison of the structures

The conformation of each of the heterocyclic rings in the structures obtained are very similar for the Na^+, K^+, and Rb^+ salts except for ring C. The conformation of ring C in the K^+ salt differs from those in the Na^+ and Rb^+ salts (see Fig. 1). This observation is consistent with the X-ray results[9] and is supported by the lack of any NOE crosspeak between H(13) and H(15B) for K^+ monensin. This cross peak exists in the NOESY spectra of Na^+ and Rb^+ monensin.

The conformation of the ethyl group is consistent throughout the series and is presumably fixed in our models by the Me(31) to H(13) medium strength NOESY interaction. In the case of the rubidium salt an additional medium strength interaction is visible between Me(31) and Me(32) resulting in a pinching across ring C and a slight change in the C(16)–C(30) dihedral angle. This change is clearly seen in the comparison of Figs. 1a and 1b with Fig. 1c.

In all of the structures the metal ion appears to have strong charge–charge or charge dipole interactions with only five oxygens (Table 4). These distances increase as expected with the larger ionic radius (Table 1). We cannot rule out the presence of a water molecule occupying a sixth octahedral coordination site. However, unlike our observations of tetronasin, we saw no evidence of this water in the NMR spectra.

In the Na^+ and K^+ salts the oxygens involved are O(2), (5), (6), (7), and (8). This changes in the rubidium salt where O(8) is replaced by O(11). Moving the chelating oxygen along the chain to accommodate the bigger ion may simply reflect an easy way to deal with the larger ionic radius. The observed metal-to-oxygen distances are in the ranges that would be expected for the hydrated alkali metal ions.[18]

Table 5 Hinge dihedral angles (°) in final structures

	Na	K	Rb
H2–H3	175.7	177.2	177.2
H3–H4	−67.9	−71.1	−71.2
H4–H5	−178.2	−178.4	−176.2
Me35–H13	58.8	56.5	61.4
C30–H17	−61.9	−66.7	−53.6
H20–H21	57.3	56.7	62.8
O11–H262	−57.6	−58.8	−61.3

Table 6 Dihedral angles and couplings about the C(20)–C(21) bond

M^+	Static angle/°	Dynamic angle/°	J_{obs}/Hz	J_{calc}/Hz[a]
Na^+	57.3	58.9	4.0	3.5
K^+	56.7	62.6	3.4	3.0
Rb^+	62.8	63.8	2.5	2.9

[a] Calculated according to the equation: $^3J_{HH} = (7.8 - 1.0\cos \Phi + 5.6\cos 2\Phi)(1 - k)$, where k is a constant to allow for relative differences in electronegativity, taken here as 0.74.

Comparison of the dihedral angles at the molecular hinges (Table 5) also reveals important changes in the overall conformation of the ligand as the ionic radius varies. Torsion angles at the flexible part of the molecule from C2 to C5 together with the O11–H262 dihedral angle show small but monotonous changes with the ionic radius. The rest of the torsion angles exhibit considerable changes (up to *ca.* 10°), which do not follow the increasing ionic radius. These hinge points are located at the middle part of the monensin backbone.

The only hinge torsion angle for which a scalar coupling constant change can readily be measured to confirm the structures is C(20)–C(21). The values for this dihedral angle given in Table 5 are those from static models. Better values for these angles for comparison with coupling constants may be obtained from an average taken from a molecular dynamics simulation. Accordingly, the molecules were allowed to evolve under NMR restraints over a 100 ps period in steps of 1 fs. The averages for the dihedral angles over this period are given in Table 6. Values of the H(20)–H(21) vicinal coupling constant were obtained from J-resolved 2D spectra and are also recorded in the Table. The couplings are seen as expected to decrease with increase in dihedral angle. To obtain a more quantitative fit the experimental values were compared with those calculated from the modified Karplus equation of Haasnoot *et al.*[19] Using a constant of 0.74 to represent electronegativity differences a satisfactory agreement was obtained (Table 6).

We conclude that monensin accommodates the increasing ionic radius by slight monotonous conformational changes near the acid group, together with some crucial concerted dihedral angle "jumps" at other hinge points. We note that the conformations of the oxygen-containing heterocyclic building blocks of the ionophore can play an important role in the overall folding of the molecule. We also note that there is the ability to change from one chelating oxygen to another to accommodate size differentials.

Molecular folding/unfolding

To simulate the unfolding of the molecule near the membrane surface, corresponding to loss of the metal ion, we ran molecular dynamics (MD) calculations of the Na^+ salt with stepwise increases in the relative permittivity (ε) from 1 to 21 (in steps of 2) (ε for water *ca.* 78 at 25 °C). This corresponds approximately to the early part of the change from the fatty interior of the membrane to the aqueous surroundings. No water molecules were included in the calculations nor were any NMR-derived distance restraints. The molecule was allowed to evolve for 10

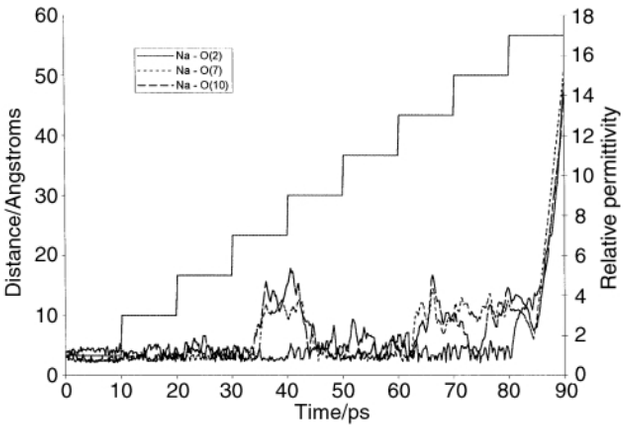

Fig. 5 Molecular dynamics derived distances for Na^+–O(2), (7) and (10) as the relative permittivity is increased in steps of 2 and the molecule allowed to evolve for 10 ps at each increment.

ps after each increase in relative permittivity. As ε was increased the binding of the carboxylate group to the sodium remained but the rest of the molecule gradually unzipped itself. The first stages were seen at around $\varepsilon = 7$ in which the first oxygens to fall away were those remote from the carboxylate group. At values of ε above 11 the ether oxygens were essentially permanently dissociated. The carboxylate oxygen eventually became dissociated at around $\varepsilon > 15$. In the presence of water with the availability of water oxygens to bind to the Na^+ ion these changes might be even more facilitated. There is no evidence from these calculations that O(7) is the first oxygen to be associated with and the last to be parted from the metal ion as had been suggested.[6] Fig. 5 plots the Na^+–O(2) and Na^+–O(7) and Na^+–O(10) distances obtained during these calculations.

These MD calculations support the idea that the first part of the monensin molecule to bind to a metal ion in the association process is the negatively charged carboxylate. Successive oxygens along the molecule then bind in turn replacing water of hydration, with the reverse happening as the metal ion is given back to the aqueous medium.

Experimental

NMR Sample preparation of monensin salts

Monensin sodium salt (10 mg) obtained from Sigma Aldrich Co. Ltd. (M5273) was dissolved in 1 cm^3 of $CDCl_3$. To this a saturated aqueous sodium/potassium/rubidium carbonate solution (*ca.* 2 cm^3) was added and the mixture was stirred vigorously for 1 hour. After stirring the mixture was allowed to settle for approximately 15 minutes. The chloroform layer was separated and filtered through a small amount of the anhydrous metal carbonate. All of the NMR samples were degassed by bubbling oxygen free nitrogen gas through the sample.

NMR Measurements

All of the spectra were obtained on a Varian Unity 500+ spectrometer at 298 K using the solvent peak at 7.27 ppm as an indirect reference to TMS at 0 ppm. The proton chemical shifts were checked against the published data with the help of COSY, TOCSY and NOESY spectra. The 2D experiments were run with 1024 complex data points in t1 and 512 complex data points in the t2 domain and 16 transients were acquired for each increment. For processing a cosine bell function was applied before transformation except for the COSY spectra for which a sine bell function was used. All spectra were zero filled once in both dimensions. The mixing time was 400 ms for NOESY experiments, which gave the best signal to noise ratio in the linear region of the nOe build up curves. For the J-resolved spectra 1024 complex data points were used in t2 and 128 data points in t1. Processing was as described above.

The distances from the NOESY cross-peak intensities were calculated by application of the isolated spin pair approximation using a geminal proton–proton distance of 1.78 Å as reference.

Molecular Mechanics

All molecular mechanics simulations were carried out on Silicon Graphics O2 and INDY computers using MSI/Biosym's CDiscover (Discover 97) software package in Insight II environment. The simulation protocols were written in Biosym's BTCL language. For the energy calculation the extensible systematic force field (ESFF) was used with 9.5 Å cut-off for van der Waals and Coulomb interactions. During the molecular dynamics calculations the velocity Verlet integrator and 1 femtosecond timestep were used. The temperature was controlled by direct velocity scaling with 10 K temperature window. The relative permittivity was distance dependent with the upper limit of 4.5 to take into account the solvent effect at this level.

The starting model was built by modification of an X-ray structure of the sodium monensin salt taken from the Cambridge Crystallographic Data Centre. The initial conformation set was created by high temperature molecular dynamics and subsequent rapid quenches. Using the starting model 50 ps MD simulations were performed at 1000 K with a 1 fs time step, and the resulting conformations were minimised and saved after every 1000 steps. The simulation was run without restraints, so the procedure was expected to discover the whole conformation space and to provide random initial conformation states.

Restrained simulated annealing was run with 55 restraints for the sodium monensin salt, 49 for the potassium monensin salt and 51 for the rubidium monensin salt (Table 3). The SA protocol was carried out with 900 K as the initial and 10 K as the final temperature. The temperature step was set to 40 K from 900 to 500 K and 7.5 K from 490 to 10 K. The duration was 500 fs from 900 to 500 K and 313 fs from 490 to 10 K at every step. Minimisation was applied after every simulated annealing in cascade manner: steepest-descent, conjugate gradient (Fletcher algorithm), Newton method (BFGS algorithm). The iteration limit was 1500 steps, and the final convergence criterion was 0.001 as maximum derivative.

In order to reveal the dynamic behaviour of our minimised static final model 100 ps restrained molecular dynamics was run at 298 K. The trajectory was updated in every 0.1 ps.

The consistency of the resulting most likely conformer with the experimental data was checked by the back calculation of the experimental data based on the trajectory of 100 ps restrained molecular dynamics simulation. The back calculation was performed using the program 'MDNOE,' written by S. Homans, which implements the RMA approach. The correlation time was estimated to 0.155 ns by the comparison of the diagonal peak and the off-diagonal peak for both the calculated and back-calculated values of their intensities.

Acknowledgements

We thank the British Council and OMFB (Budapest) for a combined grant which facilitated this work.

References

1 F. G. Riddell, *Chem. Br.*, 1992, 533.
2 F. G. Riddell, S. Arumugam and B. G. Cox, *J. Chem. Soc., Chem. Commun.*, 1987, 1890.
3 F. G. Riddell, S. Arumugam and B. G. Cox, *Biochim. Biophys. Acta*, 1988, **944**, 279.
4 F. G. Riddell and S. Arumugam, *Biochim. Biophys. Acta*, 1988, **945**, 65.
5 W. K. Lutz, F. K. Winkler and J. D. Dunitz, *Helv. Chim. Acta*, 1971, **54**, 1103.
6 W. L. Duax, G. D. Smith and P. D. Strong, *J. Am. Chem. Soc.*, 1980, **102**, 6725.

7 D. L. Ward, K. T. Wei, J. C. Hoogerheide and A. I. Popov, *Acta Crystallogr.*, *Sect. B*, 1978, **34**, 110.
8 M. Pinkerton and L. K. Steinrauf, *J. Mol. Biol.*, 1970, **49**, 533.
9 W. Pangborn, W. Duax and D. Langs, *J. Am. Chem. Soc.*, 1987, **109**, 2163.
10 P. Y. Barrans, M. Alleume and G. Jeminet, *Acta Crystallogr.*, *Sect. B*, 1982, **38**, 1144.
11 D. M. Walba, M. Hermsmeier, R. C. Haltiwanger and J. H. Noordik, *J. Org. Chem.*, 1986, **51**, 245.
12 S. Mronga, G. Müller, J. Fischer and F. G. Riddell, *J. Am. Chem. Soc.*, 1993, **115**, 8414.
13 T. Martinek, F. G. Riddell, T. J. Rutherford, S. Sareth and C. T. Weller, *J. Chem. Soc.*, *Chem. Commun.*, 1998, 1893.
14 D. L. Turner, *J. Magn. Reson.*, *Ser. B*, 1995, **108**, 137.
15 L. K. Steinrauf, M. Pinkerton and J. W. Chamberlain, *Biochem. Biophys. Res. Commun.*, 1968, **33**, 29.
16 Doctoral thesis, F. M. Vaufrey-Mary, Université Blaise Pascal, Aubière, Clermont Ferand, France, 1990.
17 F. G. Riddell, S. Arumugam, F. Fülöp and G. Bernáth, *Tetrahedron*, 1992, **48**, 4979.
18 D. T. Richens, *The Chemistry of the Aqua Ions*, Wiley, Chichester, 1997.
19 C. A. G. Haasnoot, F. A. A. M. de Leeuw and C. Altona, *Tetrahedron*, 1980, **36**, 2783.

Paper a907984j